Numerical simulation of two-phase gas-liquid flow through horizontal annulus pipe

OKU EKPENYONG NYONG[a][*]
DODEYE INA IGBONG[b]
CELESTINE EBIETO EBIETO[c]
BASSEY EKPO ENE[a]
BENJAMIN OLUWADARE[d]
ARCHIBONG ARCHIBONG ESO[e]

[a] Thermo-fluid, Combustion and Energy System Research Group, Department of Mechanical Engineering, University of Cross River State, PMB 1123, Calabar, Nigeria

[b] Department of Mechanical Engineering, University of Port Harcourt, PMB 5323 Choba, Rivers State, Nigeria

[c] Energy and Thermofluid Research Group, Department of Mechanical Engineering, Faculty of Engineering, University of Port Harcourt, PMB 5323 Choba, Rivers State, Nigeria

[d] Department of Mechanical Engineering, Ekiti State University, PMB. 5363 Ado-Ekiti, Ekiti State, Nigeria

[e] Department of Mechanical Engineering, University of Birmingham, Academic City – Dubai – United Arab Emirates, UK

Abstract Chemical, petroleum and nuclear systems are only a few of the industrial processes that utilize gas-liquid flow in annular closed channels. However, concentric horizontal annuli flow patterns have received little attention. The ability to precisely characterize two-phase flow patterns using computational techniques is crucial for the production, transportation, and optimization of designs. This current research aims to establish the accuracy of the computational fluid dynamics (CFD) model in predicting the gas-liquid flow pattern in the concentric annulus pipe and validating the flow pattern of liquid holdup with experimental results from the literature.

[*]Corresponding Author. Email: nyong.oku@uncross.edu.ng

The simulations were done on a test section of a 12.8 m length pipe with a hydraulic diameter of 0.0168 m using air and water as the working fluids. The volume of fluid (VOF) model in Ansys Fluent based on the Eulerian-Eulerian approach in conjunction with the realizable k-ε turbulence model was used to model the gas-liquid flow pattern, i.e. dispersed bubble, elongated bubble, and slug in a horizontal annulus. A comparison of the model with the experimental high-speed video images shows a reasonable agreement for the flow pattern and liquid holdup data.

Keywords: Elongated bubble flow; Gas-liquid two-phase flow; Liquid holdup; PDF; Annulus pipe; CFD modelling

Nomenclature

C_l	–	lift coefficient
C_{wl}	–	wall lubrication coefficient
D	–	pipe diameter, m
F	–	external body force, N
$\vec{F}_{\text{lift}}$	–	lift force
$\vec{F}_{td}$	–	turbulence dispersion force
$\vec{F}_{wl}$	–	wall lubrication force
$\vec{F}_{\nu m}$	–	virtual mass force
f	–	drag function
G_b	–	generation of turbulence kinetic energy due to buoyancy
G_k	–	generation of turbulence kinetic energy due to mean velocity gradients
$\vec{g}$	–	gravitational acceleration, m/s^2
$K_{pq} = K_{qp}$	–	interface exchange coefficient
$\dot{m}_{pq}$	–	mass flow rate from q to p phase, kg/s
$\vec{n}_w$	–	unit normal vector pointing away from the wall
P	–	pressure, Pa
PDF	–	probability density function
$\vec{R}_{pq}$	–	interactive force term between gas and liquid phase
Re	–	Reynolds number
u, V	–	fluid velocity, m/s
V_{SL}	–	superficial liquid velocity, m/s
V_{SG}	–	superficial gas velocity, m/s
$\vec{V}_{pq}$	–	inter-phase velocity dependent on the mass flow rate
v	–	volume, m^3
X	–	volume fraction
Y_M	–	contribution of the fluctuating dilatation in compressible turbulence to the overall dissipation rate
y^+	–	distance of the first grid cell, m

Greek symbols

ε	–	turbulent dissipation rate
μ	–	dynamic viscosity, Pa s
k	–	turbulent kinetic energy
ρ	–	density, kg/m^3

σ_k –   turbulent Prandtl number for k equation
σ_ε –   turbulent Prandtl number for ε equation
τ –   stress-strain tensor

Subscripts

i –   inner
o –   outer
q – q-th phase
p – p-th phase
L, l –   liquid
G, g –   gas
SL   –   superficial liquid
SG   –   superficial gas

Acronyms

CFD   –   Computational Fluid Dynamics
FSI   –   Fluid Structure Interaction
LIF   –   Laser-Induced Fluorescence
PIV   –   Particle Image Velocimetry
RANS   –   Reynolds-Average Navier-Stokes
RSM   –   Reynolds Stress Model
SIMPLE   –   Semi-Implicit Method for Pressure Linked Equation
VOF   –   Volume of Fluid
3D   –   3 Dimensional

1   Introduction

The transportation of two-phase media such as liquid-liquid or gas-liquid flow is common in many industries, including the chemical, nuclear, oil, and gas industries. In oil and gas facilities, flow parameters like flow pattern, liquid holdup, and pressure drop are observed and must be precisely predicted when constructing production systems as well as maintaining and running downstream facilities. These parameters enhance a reliable design for a two-phase flow pipeline and engineers can develop pipeline operation in the best possible way by having a thorough knowledge of the flow characteristic being demonstrated in a domain. Flow patterns or regimes in two-phase flow refer to the different types of fluid behaviour that can occur when two immiscible fluids (e.g., gas-liquid, liquid-liquid, etc.) flow together in a pipeline and disperse into different regions within the conduit. The flow pattern is influenced by a number of factors such as pipe geometry [1,2], fluid parameters [3–5], and the conditions of flow, which influence the flow pattern or regime [6]. The work of Ekberg *et al.* [7] studied the

impact of pipe geometry in a narrow horizontal annulus where the flow pattern was tested on two different annuli. The first pipe geometry has an inner diameter (D_i) and outer diameter (D_o) of 0.0066 m and 0.00863 m, respectively, while the second pipe geometry has an inner diameter (D_i) and outer diameter (D_o) of 0.03315 m and 0.0352 m, respectively [7]. Plug, slug, distributed bubble, churn, and other hybrid regimes were among the outcomes they got in their studies.

Numerous studies have been undertaken throughout the years to understand and gain more insight into the flow characteristics in these channels because of the significance of two-phase flow in annuli. Previous studies have shown that the centre pipe's flow obstruction causes the flow structure in the annuli configuration to differ from that of circular pipes [8, 9]. Additionally, compared to vertical flow, the gravitational effect causes the annulus with horizontal geometry to exhibit more complex flow behavior, thus, various flow regimes have distinct characteristics [9]. However, flow characteristics with unrestricted channels have been extensively studied experimentally [10,11] with the vertical [12,13] and inclined pipelines [14–16]. In horizontal annulus settings, the most common flow regimes captured by high-speed camera photography are the dispersed bubble, elongated bubble, slug, wavy slug, churn, wavy annular, and annular [8, 17]. Previous research has demonstrated that annulus eccentricity has an effect on the shape and structure of the wavy annular, elongated bubble, and annular flow regimes [8,18]. The transition from elongated bubble to dispersed bubble may occur at high liquid superficial velocities [8]. In comparison, a fully eccentric annulus, as opposed to a concentric annulus, causes the transitions between various flow regimes to happen at higher liquid and lower gas superficial velocities [8, 19]. According to other researchers, flows in totally eccentric annuli have a more well-defined structure than concentric annuli. However, the concentric annulus results in a greater pressure drop than the fully eccentric annulus [20]. Abdulkadir [2] presented an experimental and numerical investigation of gas-liquid flow in 90-degree curved pipes. The study aims to understand the effects of curvature on flow behaviour, including flow patterns, pressure drop and liquid holdup. The experiments were conducted using air and water as the gas and liquid phases, respectively. Different flow patterns, such as stratified flow, wavy stratified flow, and annular flow were observed in the curved pipes for different gas and liquid flow rates. The pressure drop and liquid holdup are measured and compared with the predicted values found from existing correlations. In addition to the experimental work, numerical simulations using the commer-

cial CFD software Star-CCM+ [20] were performed to gain further insights into the gas-liquid flow behaviour in the curved pipes. The simulations use the Eulerian-Eulerian approach to model the two-phase flow and the k-ε turbulence model to account for turbulence effects. The CFD results show good agreement with the experimental data for the flow patterns and pressure drop. The simulations also provide detailed information on the velocity and turbulence fields, revealing the complex flow behavior near the bend region [2]. Friedemann *et al.* [21] carried out a numerical study on the two-phase flow at 0–40° inclination in an eccentric annulus. They implemented the k-ω turbulence model with VOF in the Open FOAM solver [20]. In their analysis, they discovered that the horizontal case had a slug and wavy flow regime. Sultan *et al.* [22] conducted a CFD study to investigate the pressure losses and deposition velocities in horizontal annuli with different geometries and particle sizes. The study used Ansys Fluent software [23] to simulate the flow of air and particles in two different annulus geometries, namely a concentric annulus and an eccentric annulus. The particle size and the velocity of the air flow were varied to investigate their effects on the pressure losses and deposition velocities. The results of the study showed that the pressure losses in the eccentric annulus were higher than those in the concentric annulus. This was attributed to the presence of a narrow gap between the inner and outer walls of the eccentric annulus, which caused a higher resistance to flow and increased turbulence. The study also found that the pressure losses increased with increasing particle size and air flow velocity. The study also investigated the effects of different annulus geometries on the deposition velocities. The results showed that the eccentric annulus had higher deposition velocities than the concentric annulus due to the increased turbulence and particle-wall interactions in the narrow gap region. Gouidmi *et al.* [24] carried out a study on two-phase flow through an upward vertical concentric annular pipe. They investigated the effect of different flow conditions such as the gas and liquid flow rates, on the flow patterns, void fraction distribution and pressure drop. They implemented the VOF and k-ε turbulence models to simulate the flow, and the numerical results were validated against experimental data. They found out that the flow patterns in the annulus pipe were strongly influenced by the gas and liquid flow rates. The annular flow regime was observed at low gas and high liquid flow rates, while the dispersed bubble flow regime was observed at high gas and low liquid flow rates. The study also found that the void fraction distribution and pressure drop were strongly affected by the flow conditions and the flow regime. The study concluded that the numerical

model was able to predict the flow patterns and pressure drop in the annulus pipe reasonably well and provided useful insights into the behaviour of the two-phase flow in the pipe [24]. Kiran *et al.* [13] investigated two-phase flow in a vertical annulus using both experimental and modelling methods. Their model entails using two turbulence models (realizable k-ε and SST k-ω models) coupled with the VOF model to simulate the pressure drop, void fraction and flow regime. Their model predictions and the experimental result agreed rather well, with a mean error of 20%. Nyong *et al.* [17] numerically studied the CFD analysis of the liquid holdup and flow regime in an annulus section. They implemented the VOF model coupled with the turbulence model (realizable k-ε) to predict liquid holdup and dispersed bubble flow patterns. Within the condition studied at $V_{SG} = 0.18$ m/s and $V_{SL} = 1.94$ m/s, they observed the dispersed bubble flow which is composed of tiny gas bubbles dispersed throughout a continuous liquid phase. Segev *et al.* [25] worked on slug regime transitions in a two-phase flow in a horizontal rounded pipe using CFD simulations aimed to investigate the characteristics of flow pattern transitions between slug and wavy regimes in gas-liquid two-phase flows. The study used a commercial CFD code Ansys Fluent to model the two-phase flow in a horizontal round pipe. The volume of fluid (VOF) method was employed to capture the gas-liquid interface, while the k-ε turbulence model was used to simulate the turbulence effects. Their simulation results showed that the flow pattern transition from slug to wavy regime is primarily affected by the gas superficial velocity and liquid viscosity. The slug-to-wavy transition was found to occur at a lower gas velocity when the liquid viscosity was increased. Additionally, the simulations revealed that the transition from wavy to slug regime occurs at a higher gas velocity as compared to the slug-to-wavy transition.

In addition, it is established that flows in the gas phase are difficult to mathematically describe [26]. Yunpeng *et al.* [27] conducted a thorough review of the research on annular two-phase flow in vertical pipes, with a focus on investigation methodologies and advances in understanding the mechanism. Some of the experimental techniques used to measure the flow regime, void fraction and film thickness were such as the optical method [28], Laser-induced fluorescence (LIF) [29,30], particle image velocimetry (PIV), wire mesh sensor [31], gamma-absorption technique [32], etc.

Model validation on horizontal annulus configurations and flow regime features have received relatively little research. The vast majority of descriptions of flow regimes universally relied on experimental evidence [7,8,19,33], analytical models [34] and mechanistic models [4, 15, 19, 35–37], while the

flow channel unusual shapes obstructed and deformed vision, making the experiment difficult. It is important to note that most research done prior to 2000 had limitations on data and application ranges [38]. However, among the most popular tools used for examining and characterizing flow regimes in complex geometries are CFD tools. The physics of flow, accessibility of computational resources, the level of accuracy required, and the time needed for the solution – all have an impact on the fidelity of the results and the selection of turbulence model for a CFD problem. The usefulness of well-known Reynolds-averaged Navier-Stokes (RANS) turbulence models, that is the k-ε model, k-ω model, and RSM in addition to large eddy simulation (LES) for steady fluid flow *via* pipelines has considerably been investigated in literature [39–42]. This current research aims at establishing the accuracy of the CFD model in predicting the gas-liquid flow pattern in the concentric annulus pipe and validating the flow pattern liquid holdup with experimental results from the literature [8].

2 Model

2.1 Computational geometry

The model was developed using the Ansys 19.0 commercial package [23]. ANSYS 19.0 Workbench [23] offers a user-friendly and intuitive graphical interface that allows users to access and navigate through different simulation tools and workflows. It seamlessly integrated with CAD software, allowing users to import geometries directly from computer-aided design (CAD) systems and perform simulations on the CAD models. This integration streamlines the simulation setup process and ensures accurate geometry representation. It also supports multiphysics simulations, enabling users to analyse the interactions between different physical phenomena. It allows for coupling between fluid dynamics, thermal analysis, and more to accurately model real-world engineering problems. This model was actualized on an HP Intel Core I7 computer with 12 Gigabytes of RAM and a 4.7 GHz microprocessor. The geometry for the CFD model were prepared in Ansys 19.0 workbench [23]. The model has two sections. The first section is made of a stainless steel of length 2 m and the section proceeding the 2 m section is a test section, which is transparent pipe of length 10.8 m as shown in Fig. 1. The mixtures (gas and liquid) are injected separately into the test section via an inclined pipe at 90° forming a tee section at the beginning of the test section. Figure 1 depicts the geometrical parameters of
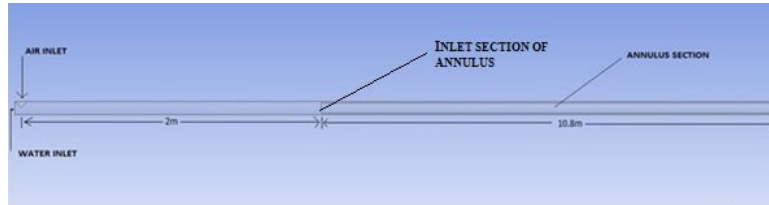
Figure 1: The side view with dimensions of the test section of the facility.

test section of the facility. Details of experimental setup of the test facility and representation of the geometrical can be found in the works of Eyo *et al.* [8]. Gas and liquid enters the 2 m pipe length through the air and water inlet port and mixing of the fluid takes place along the 2 m pipe section before advancing to the inlet section of the annulus. This arrangement is to allow for fully developed flow along the axial direction as earlier detailed in the experimental setup [43, 44]. The annulus section is made of pipe in pipe configuration. This arrangement has two PVC pipes, one with an inner pipe diameter of 0.06 m and the other with an outer pipe diameter of 0.078 m placed concentrically forming hydraulic diameter of 0.0168 m. The geometric parameters for the simulation is found in Table 1. The fluid used at the entrance are gas (air) and liquid (water) phase, which are assigned with velocities called the superficial velocities of gas and liquid respectively. The phases have been clearly defined with the primary phase as air and the secondary phase as water. The volume fraction and the density of each phase were both prescribed at the entrance. The properties of the fluid used for this simulation is found in Table 2. The pipe roughness height was

Table 1: Geometric parameters for the CFD calculation [1].

Geometrical parameter	Value
Outer pipe diameter (m)	0.0768
Inner pipe diameter (m)	0.060
Hydraulic diameter (m)	0.0168
Length of mixing section (m)	2
Length of annulus section (m)	10.8
Wall roughness height (m)	0.000015
Wall roughness constant	0.5

considered to be 0.000015 m for the wall, while the roughness constant was taken as 0.5. The gas-liquid phases were maintained at a room temperature of 15°C and atmospheric pressure of 101 325 Pa. The superficial gas and liquid velocities for the conditions studied ranges from 0.18 to 0.62 m/s and 0.28 to 1.94 m/s respectively. The time-series of area average liquid hold-up were recorded from inlet section of the annulus pipe up to about 6 m.

2.2 Mesh distribution and study

The outcome of the simulation relies greatly on the mesh characteristics. The geometry of the annulus section is a circular pipe. The variation in mesh construction is one of the primary causes of deviations in flow characterization. Mesh sensitivity is used to describe the dependence of the numerical results on the mesh size used in the simulation. The grid or mesh of points is used to discretize the domain being simulated such as a fluid domain or a solid domain. In a numerical simulation, the results are typically more accurate as the mesh size is reduced, because a finer mesh captures more details of the flow or behaviour as being simulated. However, using a very fine mesh can be computationally expensive and time-consuming, and may not always be necessary. In this study, a numerical simulation was run with different mesh densities and comparing the results to determine if the solutions are significantly affected by increasing the mesh density. This helps to identify the optimal mesh density to use for this simulation, balancing accuracy and computational efficiency. The current simulation was performed by running with a coarse mesh and gradually refining the mesh until the results converge and are no longer significantly affected by further refinement. As a result of no-slip condition, the shear flow that develops near the wall contributes to the instability of the interface and is therefore essential to the development of the overall flow. Figure 2 shows the top and side view of the annulus section; it is seen that for the present modelling a quadrilateral structured mesh was selected and refined near the inner and outer wall region and reasonably coarser mesh at the central region of the annulus [45]. The simulation was tested at conditions of superficial velocities of $V_{\mathrm{SL}} = 1.94$ m/s and $V_{\mathrm{SG}} = 0.18$ m/s, with fluid density for liquid and gas given as $\rho_L = 998.2$ kg/m^3 and $\rho_G = 1.225$ kg/m^3, respectively. The pressure was taken after the entrance length of 2 m that is at the inlet of the annulus section.

Figure 3 clearly shows the decline in pressure gradient from 25 kPa to about 14.7 kPa, where a consistency is maintained at a mesh density be-
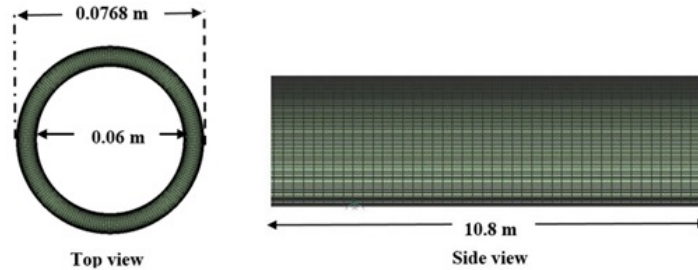
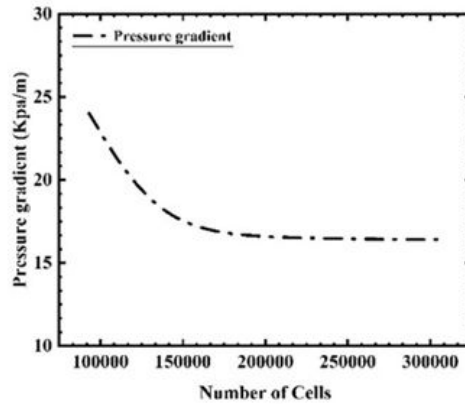Figure 2: The top and side view of the annulus section.

Figure 3: The mesh sensitivity analysis.

tween 205 000 and 306 000 cells. Further increase in the volume of cells resulted in no significant change in the pressure gradient (less than 0.4%). However, the flow solution and the integrated quantities will not be altered even if the number of mesh cells used to model the flow is increased beyond this volume of cells. Therefore, the mesh density of 205 000 cells was used in simulating the flow conditions. The mesh quality recorded an orthogonal quality of 0.998 which signifies a very good mesh. It is important to note that mesh sensitivity is just one aspect of the overall numerical simulation accuracy, and other sources of error such as boundary conditions and numerical scheme were also considered.

The y^+ was used as a guide to determine the appropriate wall modelling strategy to use in the simulation. The y^+ value in CFD modelling is determined by the distance of the first grid cell from the wall of the simulation domain, typically a solid boundary. The y^+ value is a dimensionless param-

eter used to evaluate the adequacy of the resolution of the near-wall region of a CFD simulation. It is defined as

$$y^+ = \frac{(\rho u y)}{\mu}\,, \tag{1}$$

where ρ is the fluid density, u is the velocity of the fluid, y is the size of the first grid cell. If the y^+ value is too high, the first grid cell may not be able to accurately capture the flow behaviour in the near-wall region, leading to incorrect or inconsistent results. On the other hand, if the y^+ value is too low, the simulation may become computationally expensive or unstable, as a large number of grid cells would be needed to resolve the boundary layer. Typically, for this study, a y^+ value of 1 was used for wall-resolved simulations, where the near-wall region was resolved with the grid. However, a value of $y^+ > 30$ has been the recommended standard for wall-modelled simulations, where the near-wall region is modelled using the k-ε turbulence model [23]. In the current work, a y^+ above 50 was adopted. The boundary conditions were specified at the inlet port for water and gas and at the inlet section of the annulus, while the outlet port was denoted as the pressure outlet condition. The turbulence was specified in terms of intensity and hydraulic diameter. The intensity was assumed to be 5%, while the hydraulic diameter was 0.0168 m in this case. The outlet was open to the atmosphere and hence the pressure at the outlet boundary was considered to be 0 Pa (gauge pressure). At the entrance, both the density and volume fraction of each phase were specified. The fluid properties of gas and liquid used in the simulation are given in Table 2.

Table 2: Fluid properties for the CFD simulation study.

Density of liquid (ρ_L), kg/m^3	Density of gas (ρ_G), kg/m^3	Dynamic viscosity of liquid (μ_L), kg/ms	Dynamic viscosity of gas (μ_G), kg/ms	Temperature of the fluid, $^\circ$C	Pressure, Pa	Surface tension (σ), N/m
998.2	1.225	0.000894	0.00001821	15	101325	0.07286

2.3 Computational method

The VOF model is based on the Eulerian–Eulerian approach, which is used in the current CFD simulation. The VOF model works on surface tracking methods implemented for immiscible (two-phase) fluids [46]. It can be

applied for steady or transient tracking of any gas-liquid interface. The VOF model is effectively used in this work because of its relative simplicity and low computational cost. The approach of the Eulerian-Eulerian approach is that it separately solves equations of conservation of mass and momentum for each phase, however allowing interaction between both phases through interfacial terms. However, the conservation equations can be derived by averaging the local instantaneous balance for each phase [47], or the mixture theory method could be applied [48, 49]. If the phase is q then phase volume v_q is given as

$$v_q = \int X_q \, dv, \tag{2}$$

$$\sum_{q=1}^{n} X_q = 1, \tag{3}$$

where X_q – the volume fraction phase and n signifies the number phases. In the modelling, 'q' and 'p' represent the primary phase of liquid and 'q' represents the secondary phase of gas, respectively. Assuming no mass transfer occurs; the gaseous phase is referred to as a dispersed phase, while the liquid phase is represented as a continuum, and the governing equations (continuity and momentum) for the gas phase are given by Eqs. (4)–(5) [50, 51]:

$$\frac{\partial}{\partial t} \left(\rho_q X_q \right) + \nabla \cdot \left(\rho_q X_q \vec{V}_q \right) = 0, \tag{4}$$

$$\begin{aligned}
\frac{\partial}{\partial t} \left(\rho_q X_q \vec{V}_q \right) + \nabla \cdot \left(\rho_q X_q \vec{V}_q \vec{V}_q \right) = {} & -X_q \nabla P + \nabla \cdot \overline{\tau}_q + \rho_q X_q \vec{g} \\
& + \sum_{p=1}^{n} \left(\vec{R}_{pq} + \dot{m}_{pq} \vec{V}_{pq} - \dot{m}_{qp} \vec{V}_{qp} \right) \\
& + \left(\vec{F}_q + \vec{F}_{\text{lift},q} + \vec{F}_{td,q} + \vec{F}_{wl,q} + \vec{F}_{\nu m,q} \right),
\end{aligned} \tag{5}$$

where ρ_q is the density of the q-th phase in the solution domain and $\vec{V}_q$ is the velocity of the q-th phase, P is the pressure shared by the entire phase, $\overline{\tau}_q$ is the q-th phase stress-strain tensor, $\vec{g}$ is the acceleration due to gravity, $\dot{m}_{pq}$ is the mass flow from (q to p) phase, $\vec{F}_q$ is the external body force, $\vec{F}_{lift,q}$ is the lift force, $\vec{F}_{td,q}$ is the turbulence dispersion force, $\vec{F}_{wl,q}$ is the wall lubrication force and $\vec{F}_{\nu m,q}$ is the virtual mass force which is applied upon the particle owing to the inertia of the primary mass encountered by the accelerated particle and if there are droplets entrained constantly between the 'q'(gas) and 'p'(liquid) phases, $\vec{R}_{pq}$ is an interaction force between the

gas and liquid phases, $\vec{V}_{pq}$ is the inter-phase velocity, and it is dependent on the mass flow rate.

The secondary phase (gas phase) of gas-liquid flows is assumed to form bubbles and exchange momentum with the liquid through the drag term as it passes through. The drag term, which dominates all other interfacial terms, is defined in Eq. (6) as

$$\sum_{p=1}^{n} \vec{R}_{pq} = \sum_{p=1}^{n} K_{pq} \left(\vec{V}_p - \vec{V}_q \right),$$ (6)

where $K_{pq} = K_{qp}$ is the interface exchange coefficient given as

$$K_{qp} = \frac{X_q X_p \rho_q f}{\tau_q}.$$ (7)

Here f is the drag function dependent on the Reynolds number. In contrast to the anisotropic drag law employed in this work, the bulk of drag models are isotropic in nature. This has an advantage over other drag laws in that it permits higher drag in the normal direction to the interface and lower drag in the tangential direction to the interface. When calculating the lift force, consideration is given to the liquid shear field, which acts perpendicular to the main flow direction and is proportional to the gradient of the liquid velocity field. Equation (8) gives the lift force in terms of the slip velocity and the curl of the liquid phase velocity:

$$\vec{F}_{\text{lift},g} = -C_l \rho_g X_g \left(\vec{V}_l + \vec{V}_g \right) \times \left(\nabla \times \vec{V}_l \right).$$ (8)

Compared to the drag force, the lift force is negligible, but it is significant for larger bubbles. For the model, the Eötvös number determines the lift force. This model offers some advantages in the prediction of the bubble size cross-over point at which particle distortion results in a change in the lift force sign. The liquid flow rate between the wall and the bubble is less than that between the bubble and the main flow, which results in the wall lubrication force. The wall lubrication force equation is written as

$$\vec{F}_{wl,g} = C_{wl} \rho_l X_l \left(\vec{V}_l + \vec{V}_g \right)_{\parallel} |\vec{n}_w.$$ (9)

The realizable (k-ε) turbulence model developed by Launder and Spalding [52] with standard wall functions was implemented in the Ansys code [23] to solve the flow problem. The k-ε turbulence model is an isotropic turbulence model that is well suited for modelling the gas phase in two-phase flow

because it takes into account the effects of turbulent eddies on the transport of momentum and energy. It is based on two transport equations, one for the turbulent kinetic energy (k) and the other for the rate of dissipation of the turbulent kinetic energy (ε). It is computationally efficient, making it well-suited for modelling large-scale and complex two-phase flow problems. For the current work, the k-ε turbulence model was chosen because of its robustness. It had been used by previous authors to validate flow applications [53]. In that juncture, the model is used to improve the numerical solution of flows. The simultaneous solution of two separate transport equations is made possible by two-equation turbulence models, and thus allows for the measurement of the turbulent time scale and length. The transport equations for the k-ε model are given by the following Eqs. (9) and (10) [23, 52]:

$$\frac{\partial}{\partial t}\left(\rho k\right) + \frac{\partial}{\partial x_i}\left(\rho k u_i\right) = \frac{\partial}{\partial x_j}\left[\left(\mu + \frac{\mu_t}{\sigma_k}\right)\frac{\partial k}{\partial x_j}\right] + G_k + G_b - \rho\varepsilon - Y_M + S_k \quad (10)$$

and

$$\frac{\partial}{\partial t}\left(\rho\varepsilon\right) + \frac{\partial}{\partial x_i}\left(\rho\varepsilon u_i\right) = \frac{\partial}{\partial x_j}\left[\left(\mu + \frac{\mu_t}{\sigma_\varepsilon}\right)\frac{\partial\varepsilon}{\partial x_j}\right] + C_{1\varepsilon}\frac{\varepsilon}{k}\left(G_k + C_{3\varepsilon}G_b\right)$$
$$- \ C_{2\varepsilon\rho}\frac{\varepsilon^2}{k} + S_\varepsilon \,, \tag{11}$$

where u_i are the components of velocity in x_i-direction, x_i are the Cartesian coordinates ($i = 1, 2, 3$), t is the time, G_k, G_b, Y_M are the generation of turbulence kinetic energy as a result of mean velocity gradients, generation of turbulence kinetic energy due to buoyancy, and the contribution of the fluctuating dilatation in compressible turbulence to the overall dissipation rate, respectively. $C_{1\varepsilon}$, $C_{2\varepsilon}$, and $C_{3\varepsilon}$ are constants, σ_k, and σ_ε are turbulent Prandtl numbers for k and ε, respectively, while the source terms are represented as S_k and S_ε.

In the current simulation, after the mesh has been created, the boundary condition were stated. At the walls, the conditions were assumed to be non-slip at $v = 0$, and the approach of the wall function was used. The implicit body force was enacted in the model to satisfy the equilibrium condition between body force and pressure gradient terms of the momentum equation, which also handles the convergence issues in case of partial equilibrium. A pressure-based solver was used where the governing equations were discretized adopting the finite volume method. Semi-Implicit Method for

Pressure-Linked Equations (SIMPLE) scheme was activated for pressure-velocity coupling calculations [23]. For the spatial discretization, PRESTO (Pressure Staggering Option) was adopted for pressure coupling, the second order upwind for the momentum, turbulence kinetic energy and turbulence dissipation rate. Furthermore, to save computational cost, the first order implicit scheme was adopted for the transient formulation. The inlet flow conditions were initialized using the usual initialization procedure. The liquid phase was patched throughout the entire flow domain after initiation. 100 iterations were permitted for each step, with a time step of 0.001 s, which satisfies the convergence criteria [54]. The standard convergence criterion of 0.0001 was selected for residuals of continuity, velocity (u, v, w), kinetic energy (k) and dissipation rate (ε). Flow time was used to track parameters such as volume fraction and pressure gradient. From the Ansys Fluent solver, the time series and probability density function (PDF) plots of liquid holdup were obtained. The area weighted average volume fraction distribution was captured in order to further characterize the flow pattern that was observed in the modelling. The previous studies [13] have made extensive use of PDF to describe the flow structure and calculate the fraction of liquid holdup in the spatial domains employing the kernel density function of MATLAB to plot the pattern of flow. In this present work, the kernel smoothing density function of MATLAB was adopted to describe the PDF for the CFD flow patterns.

2.4 Validation

The validation of the model started with checking the mesh quality, which is crucial in getting the right numerical solutions. The convergence behaviour was checked by initiating several runs and varying the density of cells. The pressure drop along the pipe was used as a criterion to check the convergence behaviour. The cell values of the corresponding pressure gradient are shown in Fig. 3. The numerical simulation was validated with the experimental work of Eyo *et al.* [8]. Three conditions of study were initiated with the superficial velocities displayed in Table 2. Case 1 represents the simulated data for superficial velocities for air-water at $V_{SG} = 0.18$ m/s and $V_{SL} = 1.94$ m/s, respectively. Case 2 represents the simulation data for air-water with superficial velocities of $V_{SG} = 0.21$ m/s and $V_{SL} = 0.27$ m/s, and lastly, Case 3 represents the simulation data for air-water with a superficial velocities at $V_{SG} = 0.62$ m/s and $V_{SL} = 0.28$ m/s. The test matrix for the simulation is displayed in Table 2. The study was to establish the

accuracy of the turbulent model in predicting the flow regime in an annulus concentric pipe. The VOF model in Ansys 19.0 [23] was used with the Eulerian-Eulerian approach in conjunction with the turbulence (realizable k-ε) model to simulate the gas-liquid flow pattern. The modelling was carried out on an axial length of 12.8 m as shown in Fig. 1. The entire length was calculated for a simulation time of 10 s; the time it takes for the fluid to be fully developed along the 2 m section of the pipe was ignored. The calculated volume fractions of air and water were taken on a distance of 6.01 m from the inlet to the annulus section. Results obtained from the CFD simulation show that the VOF and k-ε model are adequate to mimic the flow pattern for elongated bubble and slug flow. Slight deviations were found in PDF of liquid holdup as compared with the experimental results, which is depicted in Figs. 4–9.

Table 3: Conditions and flow regime.

Cases	Superficial velocity for liquid (V_{SL}), m/s	Superficial velocity for gas (V_{SG}), m/s	Flow regime
1	1.94	0.18	Dispersed bubble
2	0.27	0.21	Elongated flow
3	0.28	0.62	Wavy slug flow

3   Results and discussions

3.1   Dispersed bubble flow

Figure 4(a) shows the CFD contours of water volume fraction at the condition of $V_{SG} = 0.18$ m/s and $V_{SL} = 1.94$ m/s, respectively. The CFD image is taken from the point where the fluid mixture enters the annulus section up to 6.01 m along the annulus section of the pipe. In Fig. 4(a), the contour plot shows the dispersed bubble flow in a horizontal concentric annulus pipe that is characterized by the formation of small gas bubbles dispersed throughout the liquid phase. These bubbles are small in size and have a spherical or elongated shape. The bubbles tend to move in a random motion, colliding and coalescing with each other, which could lead to changes in their size and shape. The liquid phase in dispersed bubble flow occupies the majority of the pipe volume, while the gas phase is dispersed as bubbles throughout the liquid phase. This type of flow is predominant with low superficial gas velocity and higher superficial liquid velocity as reported by previous

authors [8, 17]. These bubbles are created by the breaking of the slug and the movement of elongated bubbles along the annulus section. This effect results in significant liquid holdup values along the annulus region. The shape of the bubbles can also influence their dynamics, with non-spherical bubbles experiencing different drag forces than spherical bubbles. The distribution of bubbles in the flow can affect the overall flow behaviour, as the presence of bubbles can induce turbulence and promote mixing between the phases. The dynamics of dispersed bubbles can lead to a variety of complex phenomena such as bubble coalescence, breakup, and interaction with solid surfaces. For example, bubble coalescence can lead to the formation of larger bubbles, which can alter the overall flow characteristics and reduce the mass transfer efficiency. On the other hand, bubble breakup can lead to the formation of smaller bubbles, which can increase the interfacial area and promote mixing between the phases [55–57]. Figure 4(b) depicts the video image captured from the high speed camera, which shows the formation of very small gas bubbles dispersed throughout the liquid phase. The bubbles of the CFD image look slightly larger than those of the experiment; this might be attributed to the runtime of the simulation, which if run further between 12 s and 15 s, it could have captured more details of the breakup of large bubbles.

(a)   (b)
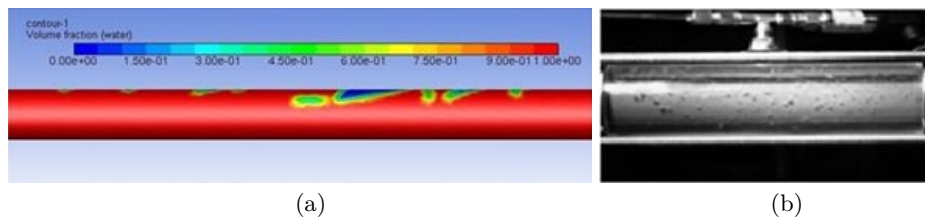
Figure 4: (a) CFD contour plot of volume fraction of water in the annulus region; (b) visual image of dispersed flow from high speed camera [1]; $V_{SG} = 0.18$ m/s and $V_{SL} = 1.94$ m/s.

The flow pattern is further characterized by using the time series of the liquid holdup for the experimental data and the PDF plots of liquid holdup generated from the CFD data. Figure 5(a) depicts the simulated variation of the liquid holdup. In Fig. 5(b), it is seen that the dispersed bubble flow exhibits a uniform oscillation of the time-varying liquid holdup between the values of 0.917 and 0.93, which is close to 1, indicating the presence of spherical bubbles scattered along a continuous liquid phase as revealed in Fig. 5(a). The liquid holdup of the dispersed gas phase (i.e. the bubbles) is

very small, while the liquid phase occupies almost the entire volume of the
flow as rightly observed by other authors [57]. When compared with the
time variation of liquid holdup in the experiment, a more steady oscilla-
tion was observed for time variation liquid holdup of about 1 signifying the
dispersed bubble in a continuous liquid phase. Figure 5(c) shows a com-
parison between the simulated CFD model and experimental PDF trend;
both the simulation and experiment showed their unimodal peak values at
liquid holdup values of 0.93 and 0.97, respectively which is eventually close
to 1. Then, the error of the CFD simulation is estimated to be 4% when
compared with the experimental data. From the plot, it is established that
the VOF model coupled with the k-ε turbulence model adequately predicts
the probability density function (PDF) trend of liquid holdup for dispersed
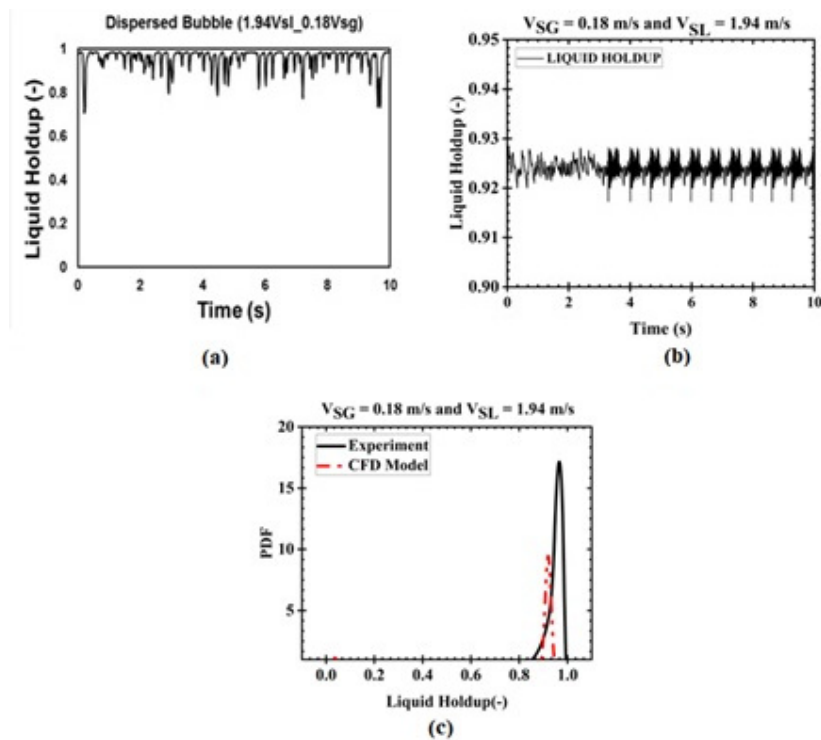bubble flow.

Figure 5: The time variation of liquid holdup and PDF trend at $V_{SG} = 0.18$ m/s and
$V_{SL} = 1.94$ m/s: (a) the measured time variation of liquid holdup, (b) PDF
trend obtained for dispersed bubble by visual image in literature [1], (c) com-
parison of PDF of simulated variation of liquid holdup with the experimental
trend for dispersed bubble flow.

3.2 Elongated bubble flow

Figure 6(a) depicts the calculated contours of liquid volume fraction for the elongated bubble at $V_{SG} = 0.27$ m/s and $V_{SL} = 0.21$ m/s. Within the region, the bubble flow is characterized by a discontinuous liquid body that fills the annulus zone and is limited at its top by gas plugs. As previously reported in the literature [57–59], at lower gas and liquid superficial velocities, this particular flow pattern is significant and is characterized by an alternating liquid body that fills the entire cross section of the annulus and gas plugs confined at the annulus top. The pattern of the formed gas plug is rightly conditioned by the annulus configuration. The elongated bubble flow is formed in a horizontal concentric annulus pipe as a result of continuous gas phase flow through a liquid phase, creating elongated bubbles. The shape of the annulus and the flow rates of the gas and liquid phases can influence the formation of elongated bubbles. At low liquid flow rates, elongated bubbles can form due to the low frequency of liquid slugs. At high gas flow rates, the gas can displace the liquid and create elongated bubbles. Additionally, the presence of obstacles or bends in the annulus can also affect the formation of elongated bubbles.

In comparison with the experimental image captured from the high speed camera in Fig. 6(b), the calculated elongated bubbles are slightly larger in shape; this might be due to the shear force acting on them in the centre of the annulus. It is seen that the VOF and k-ε model adequately predict the flow pattern for elongated bubble as compared with the video image obtained from the experiment.
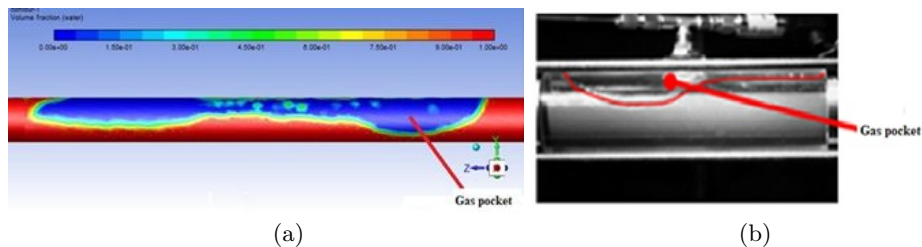

(a) (b)

Figure 6: Comparison between (a) CFD contour plot of volume fraction of water in the annulus section for elongated bubble flow and (b) visual image of elongated bubble flow from a high speed camera [1]; $V_{SG} = 0.27$ m/s and $V_{SL} = 0.21$ m/s.

The time variation of liquid holdup in the experiment and the CFD model is shown in Fig. 7. In Fig. 7(a), the time variation of liquid holdup plot in the experiment fluctuated intermittently from a crest value of 0.8 to

a crest value of 1, which indicates high closeness to liquid holdup value. This means that the annulus section is completely filled with liquid, as indicated by the higher crest value. The crest value for the simulated time-varying liquid holdup plot was observed to fluctuate between 0.1 and 0.6. It can be seen that the CFD model underestimates the time-varying liquid holdup for elongated bubble flow. In contrast to the visual appearance from the experiment, the PDF trend from the simulated data in Fig. 7(c) displays two peak values that are further apart with bimodal peak values of 0.2 and 0.6, while the experimental results demonstrate two peak values of liquid holdup of 0.7 and 1.0.
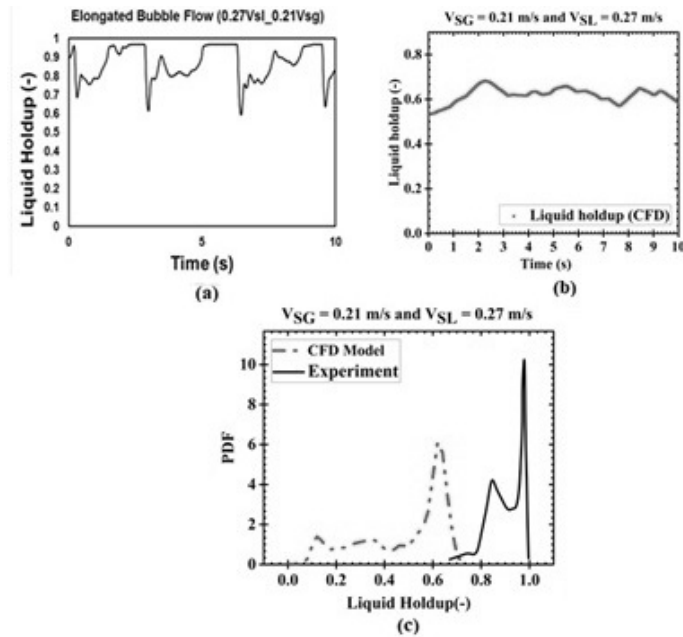

Figure 7: The time variation of liquid holdup and the PDF of liquid holdup at $V_{SG} = 0.27$ m/s and $V_{SL} = 0.21$ m/s: (a) the experimentally measured time variation of liquid holdup for elongated bubble from experiment [1]; (b) CFD simulated time variation of liquid holdup obtained for elongated bubble flow; (c) comparison of CFD and experimental PDF of liquid holdup for elongated bubble flow.

3.3   Slug flow

Figure 8(a) depicts the simulated contours of volume fraction of air-water at superficial velocities of air and water $V_{SG} = 0.62$ m/s and $V_{SL} = 0.28$ m/s, respectively. It is clear that the air phase appears in two different forms:

large and small spherical bubbles dispersed in the water phase. Large bubbles occupy almost the entire cross section of the annulus and move uniformly upwards. The liquid (water) phase appears as liquid plugs that span over the cross section of the annulus pipe, and as falling liquid films that flow downwards between the large bubbles (slug air) and the tube walls. The slugs (water) which separate the main successive bubbles contain small dispersed spherical gas bubbles. As a result of a decrease in flow holdup and increased turbulence, the liquid phase wraps itself around the inner pipe of the annulus and contains some entrained air bubbles flowing close to the top of the annulus [8]. As a result of the high gas superficial velocity, the wavy interface and stratified smooth flow are observed along the annulus section during the flow simulation. The contour phase distribution for this case shows a clear chaotic, unstable and wavy spike image, whose behaviour was reported by Roberto *et al.* [60]. A similar trend was captured from the visual (experimental) image placed in Fig. 8(b) [8]. It can be seen that the VOF and k-ε models conveniently predict the slug flow with the studied condition, showing a good agreement with the video image captured from the experiment.

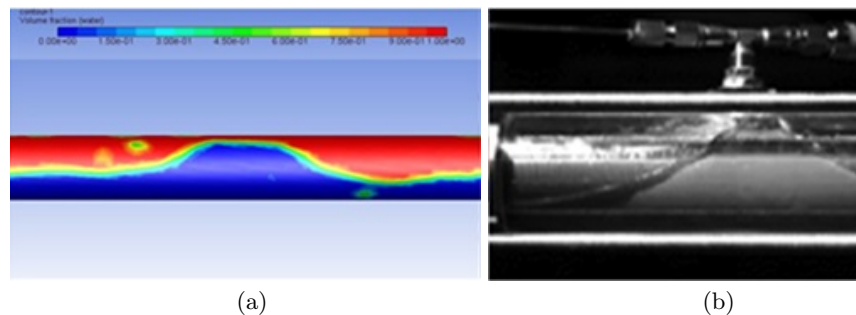(a)   (b)

Figure 8: The comparison between (a) the CFD contour plot of volume fraction of air-water along the annulus section for slug flow and (b) the visual observations from high-speed imaging of slug flow; $V_{SG} = 0.62$ m/s and $V_{SL} = 0.28$ m/s [1].

Figure 9 shows the time variation and the PDF of liquid holdup for both the model and experimental data. In Fig. 9(a), the experimental time-varying liquid holdup for slug flow is illustrated. The experiment shows a pulsating flow between the crest values of 0.3 and 1, which shows how the slug liquid body and Taylor bubble alternate with the annulus section. Figure 9(b) shows the time-varying liquid holdup for the CFD model having pulsating flow between the crest value of 0.3 and 0.5. However, Fig. 9(c) shows the

comparison of the simulated and experimental PDF of liquid holdup for slug flow. From the plot, a bimodal trend is observed for the simulated data, which is in line with the experimental data. It can be seen from the plot in Fig. 9(c) that two distinct peaks are observed from the CFD model. The first peak occurs within the liquid holdup range of 0.3–0.5, while the second peak is within the range of 0.3–0.4. The first peak was adequately predicted, falling in the same range as in the experiment, while the higher peak was underestimated compared with the experiment where it falls in the range of 0.8–0.9.
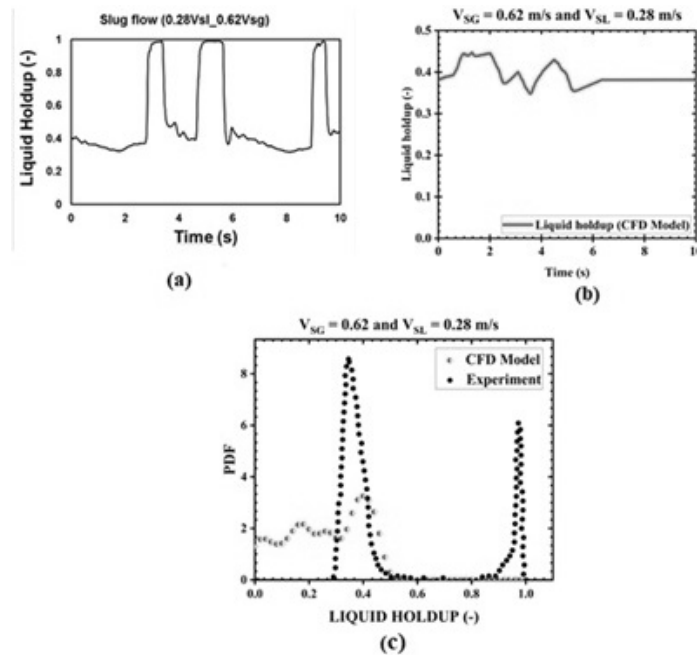

Figure 9: The time variation of liquid holdup and the PDF trend at $V_{SG} = 0.62$ m/s and $V_{SL} = 0.28$ m/s: (a) the measured time variation of liquid holdup from experiment [1]; (b) simulated time variation of liquid holdup for slug flow; (c) comparison between the CFD model and experiment for PDF of liquid holdup for slug flow.

4 Conclusions

The current work was carried out to establish the accuracy of the CFD model in predicting the flow pattern and also validate the work of Eyo *et al.* [8] in a horizontal concentric annulus pipe. This was achieved through

the use of the VOF model, which is based on Eulerian-Eulerian approach in conjunction with the turbulence model (realizable k-ε) in Ansys Fluent. Simulations were done on a 12.8 m long pipe with a hydraulic diameter of 0.0168 m using air and water as the main operating fluids. The entire length was calculated for a simulation time of 10 seconds; the time it takes for the fluid to be fully developed along the 2 m section of the pipe was ignored. The calculated volume fractions of air and water were taken on a distance of 6.01 m from the inlet to the annulus section. Three basic two-phase flow regimes were predicted for the condition of superficial velocities studied. These flow patterns were obtained by varying the superficial velocity of air and water to obtain regimes such as the elongated bubble, dispersed bubble and slug flow regimes. The validation of the model started with the checking of the mesh quality, which is crucial in getting the right numerical solutions. The convergence behaviour was checked by initiating several runs and varying the density of cells. The pressure drop along the length of the pipe was used as a criterion to check the convergence behaviour. The cell values of the corresponding pressure gradient were recorded. The validation of CFD results of two-phase flow patterns determined as a combination of time series and PDF of the liquid holdup was made with the help of an experiment of visual image capture from a high-speed camera. The PDF model was used to describe the flow structure and calculate the fraction of liquid holdup in the spatial domains employing the kernel density function of MATLAB to plot the pattern of flow. From the PDF trend results, the crest value for the simulated time-varying liquid holdup plot for elongated bubble was observed to fluctuate between 0.1 and 0.6. It can be seen that the CFD model underestimated time-varying liquid holdup for an elongated bubble flow. For slug flow the first peak was adequately predicted which falls in the same range as in the experiment and the higher peak was underestimated compared with the experiment data, where it falls in the range of 0.8–0.9. The numerical results showed a good agreement with the corresponding experimental data over a studied range of flow conditions.

Future works are underway to ensure that the turbulence (realizable k-ε) model can be used to simulate other flow regimes of liquid holdup for concentric and fully eccentric pipes at varying superficial velocities conditions and also to predict the pressure gradient of the system.

References

[1] Crawford N.M., Cunningham G., Spence S.W.T.: *An experimental investigation into the pressure drop for turbulent flow in 90 elbow bends.* Proc. Inst. Mech. Engrs. E: J. Process Mech. Eng. **221**(2007), 77–88. doi: 10.1243/0954408JPME84

[2] Abdulkadir M.: *Experimental and computational fluid dynamics (CFD) studies of gas-liquid flow in bends.* PhD thesis, Univ. Nottingham, 2011.

[3] Sarica C., Pereyra E.J.: Brito R.: *Effect of medium oil viscosity on two phase oil gas flow behavior in horizontal pipes.* In: Proc. Offshore Technology Conf., Houston, May 2013. doi: 10.4043/24048-MS

[4] Tzotzi C., Bontozoglou V., Andritsos N., Vlachogiannis M.: *Effect of fluid properties on flow patterns in two-phase gas – liquid flow in horizontal and downward pipes.* Ind. Eng. Chem. Res. **50**(2011), 2, 645–55. doi: 10.1021/ie100239v

[5] Matsubara H., Naito K.: *Effect of liquid viscosity on flow patterns of gas-liquid two-phase flow in a horizontal pipe.* Int. J. Multiphas. Flow **37**(2011), 10, 1277–1281. doi: 10.1016/j.ijmultiphaseflow.2011.08.001

[6] Waelchli S, von Roh P.R.: *Two-phase flow characteristics in gas–liquid microre-actors.* Int. J. Multiphas. Flow **32**(2006), 7, 791–806. doi: 10.1016/j.ijmultiphase flow.2006.02.014

[7] Ekberg N.P., Ghiaasiaan S.M., Abdel-Khalik S.I., Yoda M., Jeter S.M.: *Gas–liquid two-phase flow in narrow horizontal annuli.* Nucl. Eng. Des. **192**(1999), 1, 59–80. doi: 10.1016/S0029-5493(99)00078-3

[8] Eyo E.N., Lao L.: *Gas-liquid flow regimes in horizontal annulus.* J. Petrol. Sci. Eng. **175**(2019), 573–586. doi: 10.1016/j.petrol.2018.12.056

[9] Barnea D., Luninski Y., Taitel Y.: *Flow pattern in horizontal and vertical two phase flow in small diameter pipes.* Canadian J. Chem. Eng. **61**(1983), 617–20.

[10] Izwan Ismail A.S., Ismail I., Zoveidavianpoor M., Mohsin R., Piroozian A., Misnan M.S., *et al.*: *Experimental investigation of oil–water two-phase flow in horizontal pipes: Pressure losses, liquid holdup and flow patterns.* J. Petrol. Sci. Eng. **127**(2015), 409–420.

[11] Mandhane J.M., Gregory G.A., Aziz K.: *A flow pattern map for gas – liquid flow in horizontal pipes.* Int. J. Multiphas. Flow **1**(1974), 537–553.

[12] Farman Ali S., Yeung H.: *Experimental study of two-phase air–water flow in large-diameter vertical pipes.* Chem. Eng. Commun. **202**(2015), 823–842.

[13] Kiran R., Ahmed R., Salehi S.: *Experiments and cfd modelling for two phase flow in a vertical annulus.* Chem. Eng. Res. Des. **153**(2020), 201–211.

[14] Jagan V., Satheesh A.: *Experimental studies on two phase flow patterns of air–water mixture in a pipe with different orientations.* Flow Meas. Instrum. **52**(2016), 170–179.

[15] Barnea D., Shoham O., Taitel Y., Dukler A.E.: *Flow pattern transition for gas-liquid flow in horizontal and inclined pipes. Comparison of experimental data with theory.* Int. J. Multiphas. Flow **6**(1980), 217–225.

[16] Rodriguez O.M.H., Baldani L.S.: *Prediction of pressure gradient and holdup in wavy stratified liquid–liquid inclined pipe flow.* J. Petrol. Sci. Eng. **96-97**(2012), 140–151.

[17] Nyong O., Fakorede D., Ifere M., Bepaye A., Igbong D., Ebieto C., *et al.*: *CFD modelling of dispersed bubble two-phase flow in a concentric annulus pipe.* Int. Res, J. Innovat. Eng, **5**(2021), 82.

[18] Ibarra R., Nossen J., Tutkun M.: *Two-phase gas-liquid flow in concentric and fully eccentric annuli. Part I: Flow patterns, holdup, slip ratio and pressure gradient.* Chem. Eng. Sci. **203**(2019), 489–500.

[19] Lage A.C., Rommetveit R., Time R.W.: *An experimental and theoretical study of two-phase flow in horizontal or slightly deviated fully eccentric annuli.* In: Proc. IADC/SPE Asia Pacific Drilling Technology, OnePetro; 2000.

[20] Adapco C. Star-CCM+ Theory Guide. CD-adapco. 2021.

[21] Friedemann C., Mortensen M., Nossen J.: *Two-phase flow simulations at 0–4° inclination in an eccentric annulus.* Int. J. Heat Fluid Fl. **83**(2020), 108586.

[22] Sultan R.A., Rahman M.A., Rushd S., Zendehboudi S., Kelessidis V.C.J.: *CFD analysis of pressure losses and deposition velocities in horizontal annuli.* Int. J. Chem. Eng. (2019), 7068989.

[23] Fluent A. *Ansys Fluent theory guide.* Ansys Inc, USA. 2011; 15317:724-46.

[24] Hamza G., Benderradji R., Beghidja A., Tayebi T.: *Numerical study of upward vertical two-phase flow through an annulus concentric pipe.* J. Adv. Res. Fluid Mech. Therm. Sci. **58**(2020), 187–206.

[25] Sergeev V., Vatin N., Kotov E., Nemova D., Khorobrov S.J.: *Slug regime transitions in a two-phase flow in horizontal round pipe.* CFD Simulations **10**(2020), 8739.

[26] Gioia F., Hewitt G.F., Alimonti C.: *Multiphase Flow Metering: Principles and Applications. Multiphase Flow Metering: Principles and Applications.* Elsevier Sci., 2009.

[27] Xue Y., Stewart C., Kelly D., Campbell D., Gormley M.J.W.: *Two-phase annular flow in vertical pipes: A critical review of current research techniques and progress.* Water **14**(2022), 3496.

[28] Lin R., Wang K., Liu L., Zhang Y., Dong S.: *Study on the characteristics of interfacial waves in annular flow by image analysis.* Chem. Eng. Sci. **212**(2020), 115336.

[29] van Eckeveld A.C., Gotfredsen E., Westerweel J., Poelma C.: *Annular two-phase flow in vertical smooth and corrugated pipes.* Int. J. Multiphase Flow **109**(2018), 150–163.

[30] Häber T., Gebretsadik M., Bockhorn H., Zarzalis N.: *The effect of total reflection in plif imaging of annular thin films.* Int. J. Multiphase Flow **76**(2015), 64–72.

[31] Banowski M., Beyer M., Szalinski L., Lucas D., Hampel U.: *Comparative study of ultrafast X-ray tomography and wire-mesh sensors for vertical gas–liquid pipe flows.* Flow Meas. Instrum. **53**(2017), 95–106.

[32] Hanus R., Zych M., Mosorov V., Golijanek-Jędrzejczyk A., Jaszczur M., Andruszkiewicz A.J.M., *et al.*: *Evaluation of liquid-gas flow in pipeline using gamma-ray absorption technique and advanced signal processing.* Metr. Meas. Syst. **28**(2021), 145–159.

[33] Sorgun M., Osgouei R.E., Ozbayoglu M.E., Ozbayoglu A.M.: *An experimental and numerical study of two-phase flow in horizontal eccentric annuli. Energy Sources, Part A: Recovery.* Util. Environ. Eff. **35**(2013), 891–899.

[34] Osgouei R.E., Ozbayoglu E.M., Ozbayoglu M.A., Yuksel E.: *Flow pattern identification of gas-liquid flow through horizontal annular geometries.* In: Proc. SPE Oil and Gas India Conf. Exhibit. 2010.

[35] Abbasi M., Baniamerian Z.: *Analytical simulation of flow and heat transfer of two-phase nanofluid (stratified flow regime).* Int. J. Chem. Eng. (2014), 474865.

[36] Ozbayoglu M.E., Omurlu C.: *Modelling of two-phase flow through concentric annuli.* J. Petrol. Sci. Technol. **25**(2007), 1027–1040.

[37] Omurlu C., Ozbayoglu E.M.: *A new mechanistic model for two-phase flow through eccentric horizontal annulus.* In: Proc. SPE Europec/EAGE Ann. Conf. Exhib. 2006.

[38] Lahiri S., Ghanta K.: *Computational technique to predict the velocity and concentration profile for solid-liquid slurry flow in pipelines.* In: Proc. 17th Int. Conf. on Hydrotransport, Capetown 2007, 149–175.

[39] Vijiapurapu S., Cui J.: *Performance of turbulence models for flows through rough pipes.* Appl. Math. Model. **34**(2010), 1458–1466.

[40] Markatos N.C.: *The mathematical modelling of turbulent flows.* Appl. Math. Model. **10**(1986), 190–220.

[41] Kelessidis V.C., Dalamarinis P., Maglione R.: *Experimental study and predictions of pressure losses of fluids modeled as Herschel–Bulkley in concentric and eccentric annuli in laminar, transitional and turbulent flows.* J. Petrol. Sci. Eng. **77**(2011), 305–312.

[42] Sultan R.A.: *A comprehensive study on multiphase flow through pipeline and annuli using cfd approach.* Memorial University of Newfoundland; 2018.

[43] Laufer J.: *The structure of turbulence in fully developed pipe flow.* NASA, Natl. Bureau Stand., 1953.

[44] Lien K., Monty J., Chong M., Ooi A.: *The entrance length for fully developed turbulent channel flow.* In: Proc. 15th Australian Fluid Mechanics Conf., Univ. of Sydney, Sydney, 2004, 356–363.

[45] Friedemann C., Mortensen M., Nossen J.: *Gas-liquid slug flow in a horizontal concentric annulus, a comparison of numerical simulations and experimental data.* Int. J. Heat Fluid Fl. **78**(2019), 108437.

[46] Brackbill J.U., Kothe D.B., Zemach C.: *A continuum method for modeling surface tension.* J. Comput. Phys. **100**(1992), 335–354.

[47] Anderson T.B., Jackson R.: *Fluid mechanical description of fluidized beds. Equations of motion.* Ind. Eng. Chem. Fund. **6**(1967), 527–539.

[48] Atkin R.J., Craine R.E.: *Continuum theories of mixtures: Applications.* IMA J. Appl. Math. **17**(1976), 153–207.

[49] Bowen R.: *Continuum physics* Vol. 4. 1976.

[50] Dakshinamoorthy D., Dai Y., Agrawal M.: *CFD modeling of bubbly, slugand annular flow regimes in vertical pipelines.* In: Proc. Offshore Technology Conf., Houston, 2013, 6–9.

[51] Manual U.J.T.G. Ansys Fluent 12.0. 2009.

[52] Launder B.E., Spalding D.B.: *The numerical computation of turbulent flows.* In: Numerical Prediction of Flow, Heat Transfer, Turbulence and Combustion (S.V. Patankar, A. Pollard, A.K. Singhal, S.P. Vanka, Eds.), Pergamon, 1983, 96–116.

[53] Fathi Roudsari S., Turcotte G., Dhib R., Ein-Mozaffari F.: *CFD modeling of the mixing of water in oil emulsions.* Comput. Chem. Eng. **45**(2012), 124–136.

[54] Kiran R., Ahmed R., Salehi S.J.: *Experiments and cfd modelling for two phase flow in a vertical annulus.* **153**(2020), 201–211.

[55] Renze P., Buffo A., Marchisio D.L., Vanni M.: *Simulation of coalescence, breakup, and mass transfer in polydisperse multiphase flows.* Chem. Ing. Tech. **86**(2014), 1088–1098.

[56] Luewisutthichat W., Tsutsumi A., Yoshida K.: *Bubble characteristics in multi-phase flow systems: Bubble sizes and size distributions.* J. Chem. Eng. Japan **30**(1997), 461–466.

[57] Deendarlianto A.M., Widyaparaga A., Dinaryanto O., Khasani I.: *CFD studies on the gas-liquid plug two-phase flow in a horizontal pipe.* J. Petrol.Sci. Eng. **147**(2016), 779–787.

[58] Julia J.E., Ozar B., Dixit A., Jeong J.-J., Hibiki T., Ishii M.: *Axial development of flow regime in adiabatic upward two-phase flow in a vertical annulus.* J. Fluids Eng. **131**(2009), 021302.

[59] Caetano E.F., Shoham O., Brill J.P.: *Upward vertical two-phase flow through an annulus — Part II: Modeling bubble, slug, and annular flow.* J. Energ. Res. Technol. **114**(1992), 14–30.

[60] Ibarra R., Nossen J., Tutkun M.: *Two-phase gas-liquid flow in concentric and fully eccentric annuli. Part II: Model development, flow regime transition algorithm and pressure gradient.* Chem. Eng. Sci. **203**(2019), 501–510.